

Exploring the Electronic and Optical Properties of $\text{Cu}(\text{In},\text{Ga})\text{Se}_2$

Rongzhen Chen

Supervisor: Clas Persson

Department of Materials Science and Engineering
Royal Institute of Technology, Stockholm SE-10044, Sweden

06-March-2015



Outline

1 Background

2 Motivation

3 Computational methods

4 Results

- Paper 1: parameterization of energy bands for $\text{CuIn}_{1-x}\text{Ga}_x\text{Se}_2$
- Paper 2: analysis of density-of-states (DOS) and carrier concentration
- Paper 3: dielectric function for $\text{CuIn}_{0.5}\text{Ga}_{0.5}\text{Se}_2$

5 Summary

6 Future perspectives

7 Acknowledgements

1 Background

2 Motivation

3 Computational methods

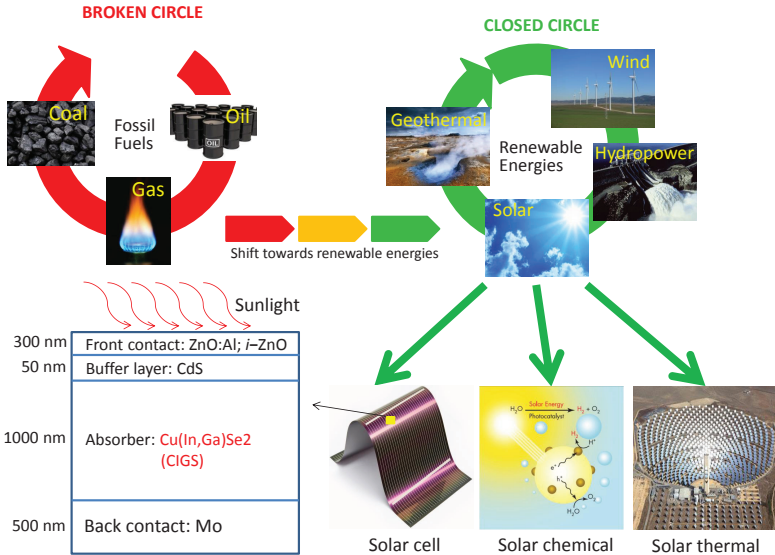
4 Results

5 Summary

6 Future perspectives

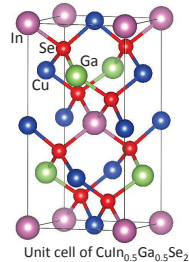
7 Acknowledgements

Which field and material am I working on?



Why Cu(In,Ga)Se₂?

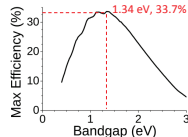
CIS = CuInSe₂
CGS = CuGaSe₂
CIGS = Cu(In, Ga)Se₂ = CuIn_{1-x}Ga_xSe₂



Unit cell of CuIn_{0.5}Ga_{0.5}Se₂

Advantages of CIGS:

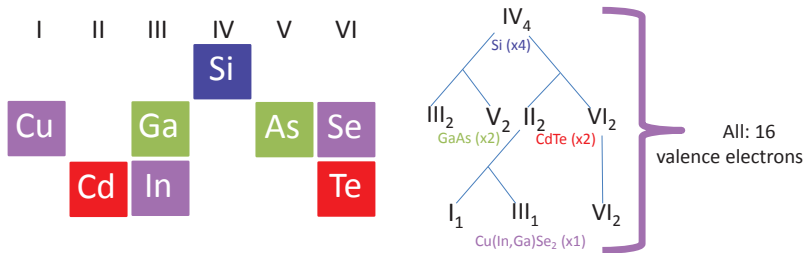
1. Tunable band-gap (1.0 to 1.7 eV)
2. Efficiency 23.3% in the lab
3. Higher absorption coefficient
→ thinner → lower cost and flexible



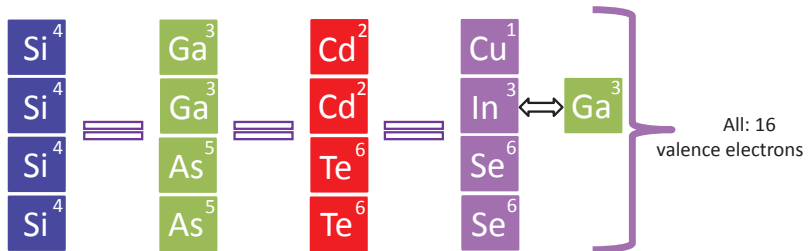
The Shockley-Queisser limit for the efficiency of a solar cell.

CIGS is doing well in the Building-integrated photovoltaics market.

Where does Cu(In,Ga)Se₂ come from?



A series of cation mutations where total number of valence electrons is the same and it keeps the charge neutral in the compound.



1 Background

2 Motivation

3 Computational methods

4 Results

5 Summary

6 Future perspectives

7 Acknowledgements

Which aspects of Cu(In,Ga)Se₂ have I been working on?

- Electronic structure

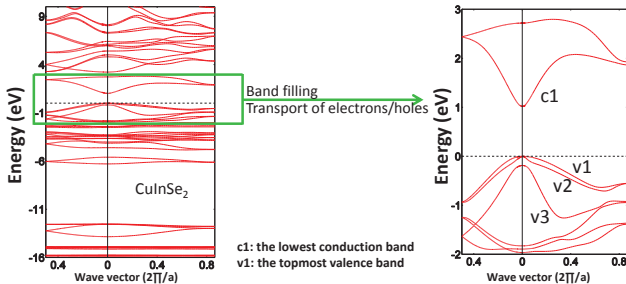
- Energy bands of CuInSe₂, CuIn_{0.5}Ga_{0.5}Se₂, and CuGaSe₂ are calculated by means of theoretical calculations. Parameterization of the lowest conduction (CB) and the three uppermost valence bands (VBs) are explored based on the calculated energy bands.
- Analysis of density-of-states (DOS) and carrier concentration based on the parameterization.

- Optical properties

- Dielectric function of CuIn_{0.5}Ga_{0.5}Se₂ are explored by means of theoretical calculations. The band-to-band optical transitions are analyzed. The electronic origins of the observed interband critical points of the optical response are discussed.

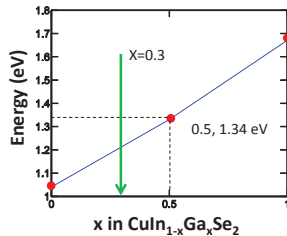
Motivation for the parameterization

By understanding the electronic properties one can understand many of the fundamental material properties.



1. Less study on CuIn_{0.5}Ga_{0.5}Se₂.

2. Commercially interesting: CuIn_{0.7}Ga_{0.3}Se₂, CuIn_{0.5}Ga_{0.5}Se₂ indicates how CIGS behaves when alloying In and Ga.



Motivation for analysis of DOS and carrier concentration

- Better analyze the impact on DOS as well as carrier concentration taking into account the non-parabolicity of the energy bands.
- Help experimentalists to reproduce DOS from energy-dependent DOS mass. Further, they can use the DOS to calculate other properties, such as carrier concentration.

Motivation for calculation of dielectric function

Absorption coefficient can be calculated by dielectric function directly. The absorption depth is given by the inverse of the absorption coefficient. That means that the material which has higher absorption coefficient uses thinner layer to absorb the same amount of light than the material which has lower absorption coefficient.

$$\alpha^{ii}(\omega) = \frac{\sqrt{2}\omega}{c} \left[\sqrt{\varepsilon_1^{ii}(\omega)^2 + \varepsilon_2^{ii}(\omega)^2} - \varepsilon_1^{ii}(\omega) \right]^{1/2}. \quad (1)$$

Here,

$$\varepsilon_2^{\alpha\beta}(\omega) = \frac{\hbar e^2}{\pi m^2 \omega^2} \sum_{cv} \int d\mathbf{k} \underbrace{< \Psi_{c\mathbf{k}} | p^\alpha | \Psi_{v\mathbf{k}} >}_{optical\ matrix\ element} < \Psi_{v\mathbf{k}} | p^\beta | \Psi_{c\mathbf{k}} > (f(\varepsilon_{c\mathbf{k}}) - f(\varepsilon_{v\mathbf{k}})) \delta(\varepsilon_{c\mathbf{k}} - \varepsilon_{v\mathbf{k}} - \omega). \quad (2)$$

$$\varepsilon_1^{\alpha\beta}(\omega) = \delta_{\alpha\beta} + \frac{2}{\pi} \mathbf{P} \int_0^\infty \frac{\omega' \varepsilon_2^{\alpha\beta}(\omega')}{\omega'^2 - \omega^2} d\omega'. \quad (3)$$

Motivation for calculation of dielectric function

- Help experimentalists to understand the dielectric function spectrum.
- Understand details in the optical transition for these types of materials.

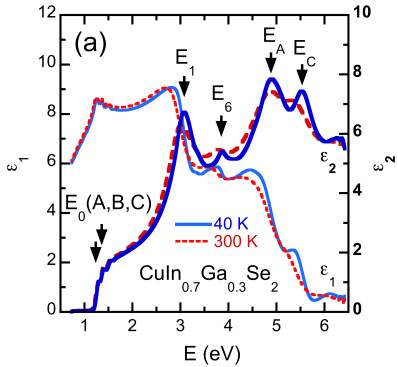


Figure 1 : The real (ϵ_1) and imaginary (ϵ_2) part of dielectric function spectra.

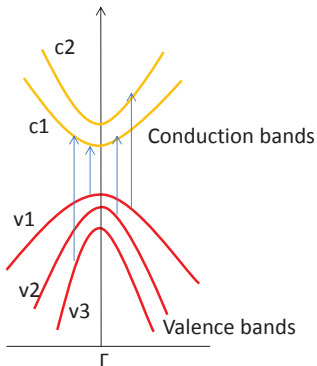


Figure 2 : Energy bands.

- 1 Background
- 2 Motivation
- 3 Computational methods
- 4 Results
- 5 Summary
- 6 Future perspectives
- 7 Acknowledgements

Density functional theory (DFT)

DFT-based modeling is extremely successful in many-body systems.

- DFT was introduced by Hohenberg and Kohn in 1964. Kohn and Pople were awarded Chemistry Nobel Prize in 1998.
- Around 20,000 papers per year.

DFT says that ground-state total energy E_{total} can be determined from the ground-state charge density $\rho(\mathbf{r})$ instead of many-electron wavefunction $\Psi(\mathbf{r}_1, \mathbf{r}_2, \dots, \mathbf{r}_N)$. Thus, total energy can be written as $E_{total}[\rho(\mathbf{r})]$. However, we do not have explicit form for $E_{total}[\rho(\mathbf{r})]$.

Here,

$$\rho(\mathbf{r}) = \int d^3r_2 \int d^3r_3 \cdots d^3r_N |\Psi(\mathbf{r}, \mathbf{r}_2, \dots, \mathbf{r}_N)|^2. \quad (4)$$

Kohn-Sham (KS) Equation

Total Energy can be written as

$$E_{total}[\rho] = T_0[\rho] + V_H[\rho] + V_{ext}[\rho] + E_{xc}[\rho]. \quad (5)$$

The single-particle KS equation is derived as

$$\left(-\frac{\nabla^2}{2} + V^{KS}(\mathbf{r}) \right) \psi_i^{KS}(\mathbf{r}) = \epsilon_i^{KS} \psi_i^{KS}(\mathbf{r}). \quad (6)$$

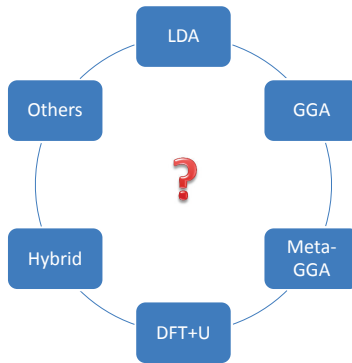
The $V^{KS}(\mathbf{r})$ is given as

$$V^{KS}(\mathbf{r}) = V_{ext}(\mathbf{r}) + \int d\mathbf{r}' \frac{\rho(\mathbf{r}')}{|\mathbf{r} - \mathbf{r}'|} + \underbrace{\frac{\delta E_{xc}}{\delta \rho(\mathbf{r})}}_{V_{xc}(\mathbf{r})}. \quad (7)$$

Here

$$\rho = \sum |\Psi_i^{KS}(\mathbf{r})|^2. \quad (8)$$

Different exchange-correlation potentials $V_{xc}(\mathbf{r})$



In our calculations, we took the GGA+U_d(Cu), that is U value on *d*-states of Cu. This method was proved to improve the effective mass, that is curvature of energy band.

1 Background

2 Motivation

3 Computational methods

4 Results

- Paper 1: parameterization of energy bands for $\text{CuIn}_{1-x}\text{Ga}_x\text{Se}_2$
- Paper 2: analysis of density-of-states (DOS) and carrier concentration
- Paper 3: dielectric function for $\text{CuIn}_{0.5}\text{Ga}_{0.5}\text{Se}_2$

5 Summary

6 Future perspectives

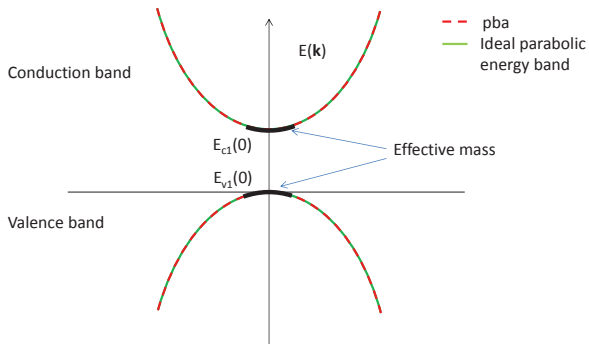
7 Acknowledgements

Paper 1: parabolic band approximation (pba)

The parabolic approximation of ellipsoidal energy bands is expressed

$$E_j^{pb}(\mathbf{k}) = E_j(\mathbf{0}) \pm \left[\frac{\tilde{\mathbf{k}}_x^2 + \tilde{\mathbf{k}}_y^2}{m_j^{xy}} + \frac{\tilde{\mathbf{k}}_z^2}{m_j^z} \right] \quad (9)$$
$$m^{ab} = \pm \hbar^2 / (\partial^2 E(\mathbf{k}) / \partial k_a \partial k_b).$$

In the case of ideal parabolic energy band, the pba can describe energy band perfectly.

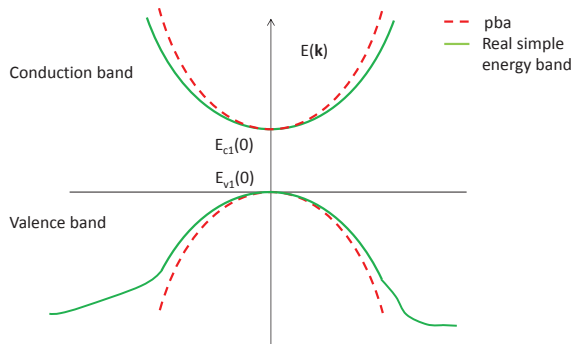


Paper 1: parabolic band approximation (pba)

The parabolic approximation of ellipsoidal energy bands is expressed

$$E_j^{pb}(\mathbf{k}) = E_j(\mathbf{0}) \pm \left[\frac{\tilde{\mathbf{k}}_x^2 + \tilde{\mathbf{k}}_y^2}{m_j^{xy}} + \frac{\tilde{\mathbf{k}}_z^2}{m_j^z} \right] \quad (10)$$
$$m^{ab} = \pm \hbar^2 / (\partial^2 E(\mathbf{k}) / \partial k_a \partial k_b).$$

The parabolic approximation is valid in the vicinity of the Γ -point. However, away from the Γ -point, it fails to describe the energy dispersion.

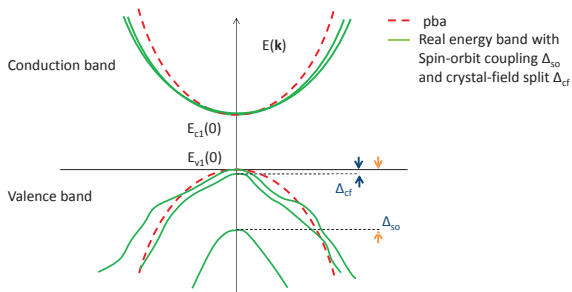


Paper 1: parabolic band approximation (pba)

The parabolic approximation of ellipsoidal energy bands is expressed

$$E_j^{pb}(\mathbf{k}) = E_j(\mathbf{0}) \pm \left[\frac{\tilde{\mathbf{k}}_x^2 + \tilde{\mathbf{k}}_y^2}{m_j^{xy}} + \frac{\tilde{\mathbf{k}}_z^2}{m_j^z} \right] \quad (11)$$
$$m^{ab} = \pm \hbar^2 / (\partial^2 E(\mathbf{k}) / \partial k_a \partial k_b).$$

Considering spin-orbit coupling and crystal-field split, the energy band becomes very complicated. The parabolic approximation is valid in the very vicinity of the Γ -point.



Paper 1: full band parameterization (fbp)

$$\begin{aligned} E_j(\mathbf{k}) = & E_j^{pb}(\mathbf{k}) + E_j^0 + \Delta_{j,1} \left(\delta_{j,1}^2 \left(\frac{\tilde{\mathbf{k}}_x^4 + \tilde{\mathbf{k}}_y^4}{m_0^2} \right) + \delta_{j,2}^2 \left(\frac{\tilde{\mathbf{k}}_x^2 \tilde{\mathbf{k}}_y^2}{m_0^2} \right) + 1 \right)^{1/2} \\ & + \Delta_{j,2} \left(\delta_{j,3}^3 \left(\frac{\tilde{\mathbf{k}}_x^6 + \tilde{\mathbf{k}}_y^6}{m_0^3} \right) + \delta_{j,4}^3 \left(\frac{\tilde{\mathbf{k}}_x^2 \tilde{\mathbf{k}}_y^4 + \tilde{\mathbf{k}}_x^4 \tilde{\mathbf{k}}_y^2}{m_0^3} \right) + 1 \right)^{1/3} \\ & + \Delta_{j,3} \left(\delta_{j,5}^2 \left(\frac{\tilde{\mathbf{k}}_z^4}{m_0^2} \right) + 1 \right)^{1/2} + \Delta_{j,4} \left(\delta_{j,6}^3 \left(\frac{\tilde{\mathbf{k}}_z^6}{m_0^3} \right) + 1 \right)^{1/3} \\ & + \Delta_{j,5} \left(\delta_{j,7}^2 \left(\frac{\tilde{\mathbf{k}}_x^2 \tilde{\mathbf{k}}_z^2 + \tilde{\mathbf{k}}_y^2 \tilde{\mathbf{k}}_z^2}{m_0^2} \right) + 1 \right)^{1/2} \\ & + \Delta_{j,6} \left(\delta_{j,8}^3 \left(\frac{\tilde{\mathbf{k}}_x^4 \tilde{\mathbf{k}}_z^2 + \tilde{\mathbf{k}}_y^4 \tilde{\mathbf{k}}_z^2}{m_0^3} \right) + \delta_{j,9}^3 \left(\frac{\tilde{\mathbf{k}}_x^2 \tilde{\mathbf{k}}_z^4 + \tilde{\mathbf{k}}_y^2 \tilde{\mathbf{k}}_z^4}{m_0^3} \right) + \delta_{j,10}^3 \left(\frac{\tilde{\mathbf{k}}_x^2 \tilde{\mathbf{k}}_y^2 \tilde{\mathbf{k}}_z^2}{m_0^3} \right) + 1 \right)^{1/3} \end{aligned} \tag{12}$$

Paper 1: parameterization of band structure for CIGS

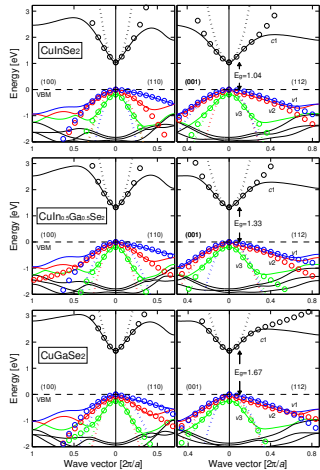


Figure 3 : Electronic band structure along four directions. The circles are the results of the fbp, the dotted lines represent the pba, and the solid lines represent the theoretical calculation.

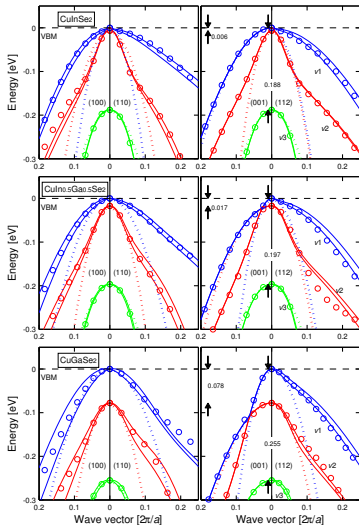


Figure 4 : Close-up of the right figure.

Paper 1: non-parabolicity of the energy bands

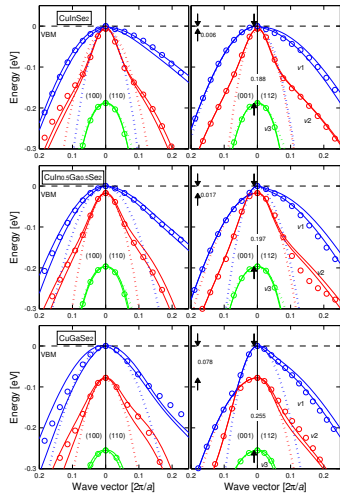


Figure 5 : Close-up of electronic band structure. The circles are the results of the fbp, the dotted lines represent the pba, and the solid lines represent the theoretical calculation.

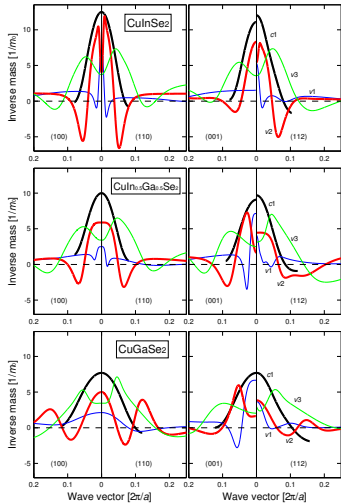


Figure 6 : Inverse of effective electron and hole masses in the four symmetry directions for CuIn_{1-x}Ga_xSe₂ ($x = 0, 0.5$, and 1).

Paper 1: non-parabolicity of the energy bands

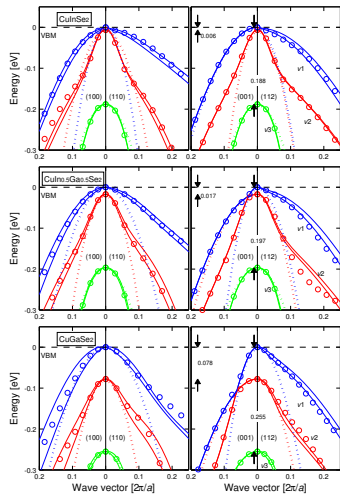


Figure 7 : Close-up of electronic band structure. The circles are the results of the fbp, the dotted lines represent the pba, and the solid lines represent the theoretical calculation.

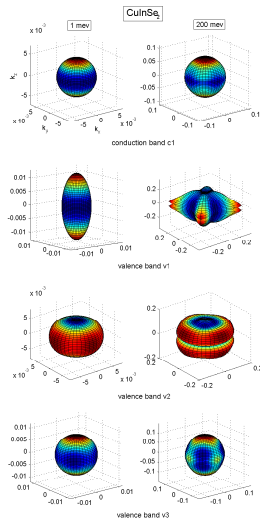


Figure 8 : Constant energy surfaces for the lowest CB and three uppermost VBs in CuInSe₂.

Paper 2: density-of-states (DOS)

In the case of the pba, the density-of-states can be written as

$$g_j^{pba}(E) = \frac{1}{2\pi^2} \left(\frac{2m_j^{DOS}}{\hbar^2} \right)^{3/2} \sqrt{|E - E_j(\mathbf{0})|}. \quad (13)$$

In order to take advantage of the simple **Eq. 13** for the non-parabolic energy bands, the energy-dependent DOS mass ($m_{v/c}^{DOS}$) is defined as

$$g_{v/c}(E) = \sum_j g_j(E) = \frac{1}{2\pi^2} \left(\frac{2m_{v/c}^{DOS}(E)}{\hbar^2} \right)^{3/2} \sqrt{|E - E_{v1/c1}(\mathbf{0})|}. \quad (14)$$

Paper 2: density-of-states (DOS) and DOS mass

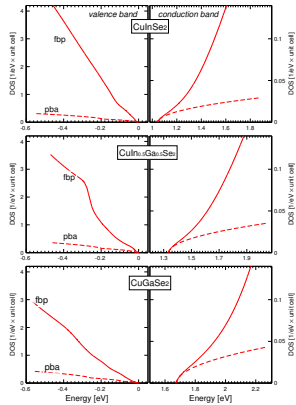


Figure 9 : Total DOS of the VBS and CB. The solid lines show the results based on the fbp, and the dashed lines represent the results based on the pba.

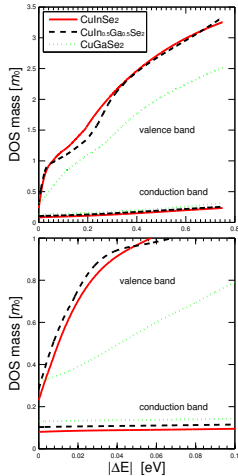


Figure 10 : DOS mass $m_{v/c}^{DOS}$.

Paper 2: intrinsic carrier concentration

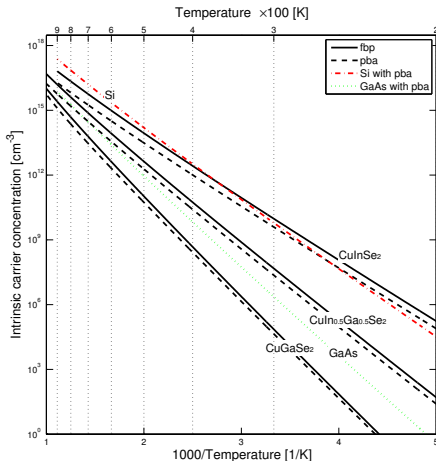
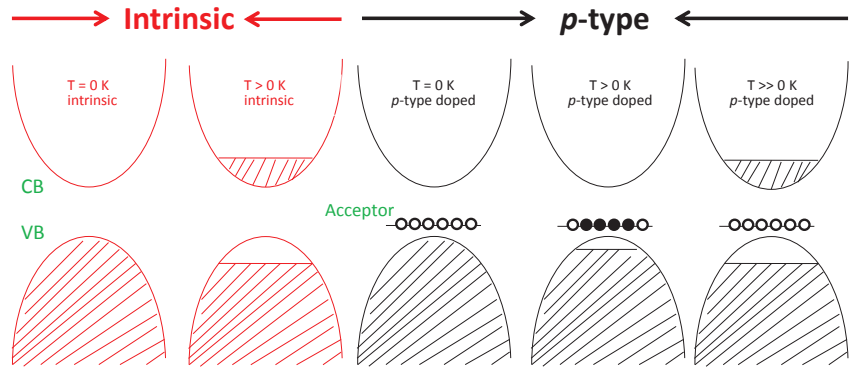


Figure 11 : Intrinsic carrier concentration as function of temperature. For comparison, the theoretical results for GaAs and Si using the pba are given.

Paper 2: carrier concentration in different temperatures



Paper 2: carrier concentration in *p*-type for CIGS

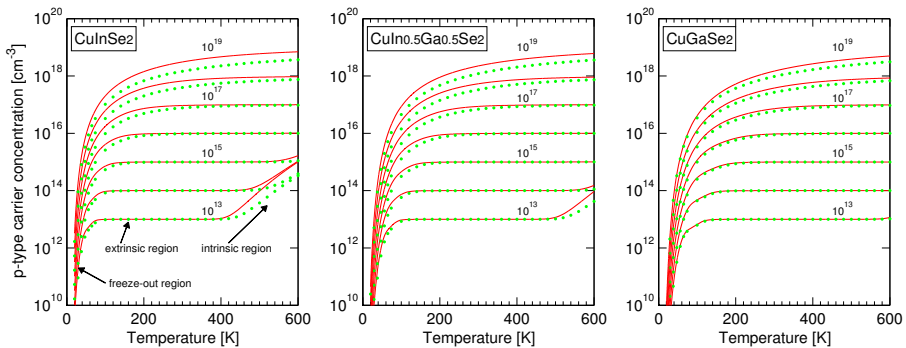


Figure 12 : Free carrier concentration as function of the temperature in *p*-type for CuInSe₂, CuIn_{0.5}Ga_{0.5}Se₂, and CuGaSe₂. The effective doping concentration $N_A = 10^{13}, 10^{14}, 10^{15}, \dots$, and $10^{19} \text{ acceptors cm}^{-3}$ are considered. Solid and dotted lines represents the fbp and the pba, respectively.

Paper 3: dielectric function for $\text{CuIn}_{0.5}\text{Ga}_{0.5}\text{Se}_2$

Absorption coefficient can be calculated by dielectric function directly. The absorption depth is given by the inverse of the absorption coefficient.

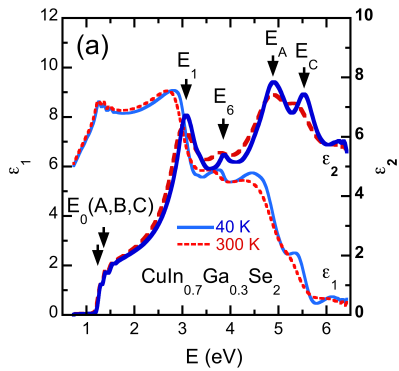


Figure 13 : The real (ϵ_1) and imaginary (ϵ_2) part of dielectric function spectra for $\text{CuIn}_{0.7}\text{Ga}_{0.3}\text{Se}_2$ at 40 K (solid blue line) and 300 K (dashed red lines). Four prominent critical point (CP) features are shown.

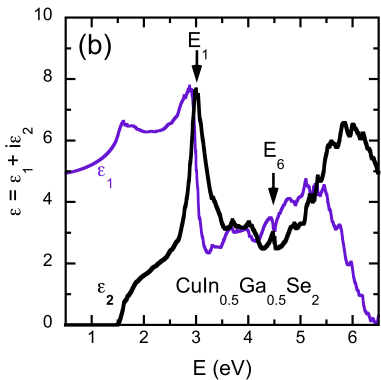


Figure 14 : The dielectric function spectra for $\text{CuIn}_{0.5}\text{Ga}_{0.5}\text{Se}_2$ calculated by FPLAPW method at 0 K. The major CP features are identified.

Paper 3: interband critical point (CP)

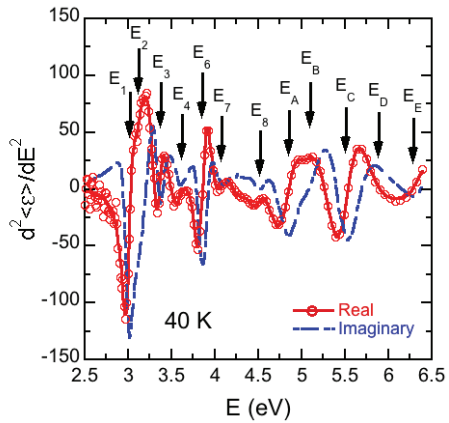


Figure 15 : Energies of each interband CP are indicated by arrows and labeled in a numeric and alphabetic order.

Paper 3: analysis of the imaginary part of dielectric function

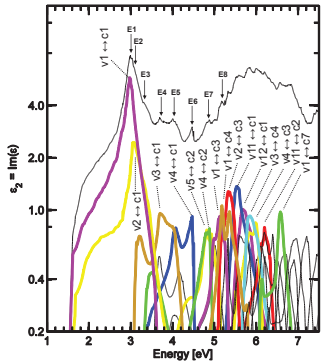


Figure 16 : Band-to-band analysis of the contribution to the total ϵ_2 spectrum. The vertical axis is in the log scale.

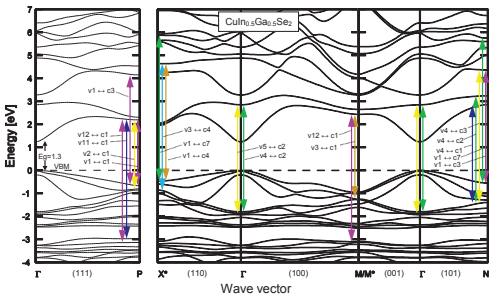


Figure 17 : The calculated electronic band structure of $\text{CuIn}_{0.5}\text{Ga}_{0.5}\text{Se}_2$ where the CPs are identified along the main symmetry directions.

- 1 Background
- 2 Motivation
- 3 Computational methods
- 4 Results
- 5 Summary
- 6 Future perspectives
- 7 Acknowledgements

Summary

- Paper 1:
 - The energy dispersions of the three uppermost VBs are strongly anisotropic and non-parabolic even very close to the Γ -point VBM.
 - The full band parameterization is valid around 0.5 eV below VBM and 0.5 eV above the conduction band minimum (CBM).
 - All the three $CuIn_{1-x}Ga_xSe_2$ ($x = 0, 0.5$, and 1.0) compositions show comparable \mathbf{k} -dependency of their effective hole masses.
- Paper 2:
 - An energy-dependent DOS mass is introduced, and it can be utilized to describe the carrier concentration and the Fermi energy using traditional equations for the DOS.
 - The transition from the freeze-out region to the extrinsic region occurs well below the room temperature for uncompensated acceptor concentration below around 10^{17} cm^{-3} , whereas for higher concentrations, not all acceptors are ionized at $T = 300 \text{ K}$. Thus, a more correct description of the energy dispersions is needed.

- Paper 3:
 - The dielectric function calculated by our theoretical method shows a good agreement with the result of experiment.
 - Electronic origins of the observed critical-point (CP) features are discussed based on our theoretical calculations.
 - The pairs of valence and conduction bands along the main symmetry directions of Brillouin zone are suggested for the major CP features based on our theoretical calculations.

- 1 Background
- 2 Motivation
- 3 Computational methods
- 4 Results
- 5 Summary
- 6 Future perspectives
- 7 Acknowledgements

Future perspectives

- The cost and scarcity of indium in the CIGS device is a problem, and copper zinc tin selenide/sulfide (CZT(S,Se)) can therefore be alternative to CIGS due to the low cost and non-toxicity elements.

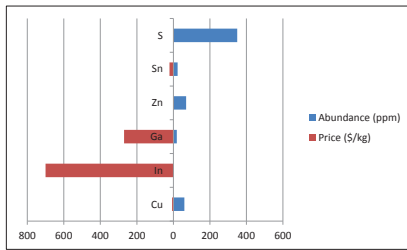


Figure 18 : Abundance and price of Cu, In, Ga, S, Sn, and Zn in Earth's crust (parts per million (ppm) in mass; 10,000 ppm = 1%).

- If there are other similar materials that are of interest. CIGS and CZT(S,Se) can be considered to be in a class denoted as Cu-XY-chalcogenide, where X and Y are two cation elements that replace the group-III In or Ga in CIGS.

- 1 Background
- 2 Motivation
- 3 Computational methods
- 4 Results
- 5 Summary
- 6 Future perspectives
- 7 Acknowledgements

Acknowledgements

- I would like to express my sincere appreciation to my supervisor Prof. Clas Persson for his academic encouragement and professional guidance.
- I would like to thank all the group colleagues in Stockholm and Oslo for helpful research discussions and chatting. I would like to thank all other people at the Department of Material Sciences and Engineering at KTH for creating a nice working atmosphere.
- The China Scholarship Council, the Swedish Energy Agency, the Swedish Research Council, Stiftelsen Axel Hultgrens fond, Olle Erikssons stiftelse for materialteknik, and KTH Computational Science and Engineering Centre (KCSE) are acknowledged for financial support.

Thank you for your attention!

Rongzhen Chen
Rongzhen.Chen@mse.kth.se

Full-potential linearised augmented-plane wave (FPLAPW)

Unit cell is divided into two regions: one is sphere region called muffin tin (MT) region, which is defined by the center of atom, but non-overlap each sphere; the remaining region is called interstitial (I) region.

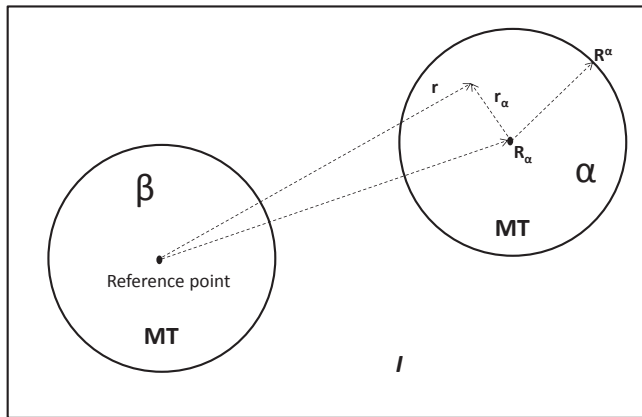


Figure 19 : Partition of the unit cell.

The KS wavefunction can be expanded by a set of basis functions

$$\Psi_{i,\mathbf{k}}^{KS}(\mathbf{r}) = \sum_{\mathbf{G}}^{N_G} C_{i,\mathbf{k}+\mathbf{G}} \phi_{\mathbf{k}+\mathbf{G}}^{LAPW}(\mathbf{r}). \quad (15)$$

Here

$$\phi_{\mathbf{k}+\mathbf{G}}^{LAPW}(\mathbf{r}) = \begin{cases} \frac{1}{\sqrt{\Omega}} e^{i(\mathbf{k}+\mathbf{G})\mathbf{r}} & \text{if } \mathbf{r} \in I \\ \sum_{\alpha} \sum_{\ell m} f_{\ell m}(r_{\alpha}, \mathbf{k} + \mathbf{G}, \epsilon_{\ell, \alpha}) Y_{\ell m}(\hat{\mathbf{r}}_{\alpha}) & \text{if } r_{\alpha} \in MT. \end{cases} \quad (16)$$

The potential in the FPLAPW method is also divided into two regions, the MT region and the I region.

$$V(\mathbf{r}) = \begin{cases} \sum_{\mathbf{G}} V_{\mathbf{G}} e^{i\mathbf{Gr}} & \text{if } \mathbf{r} \in I \\ \sum_{\ell m} V_{\ell m}^{\alpha}(r_{\alpha}) Y_{\ell m}(\hat{\mathbf{r}}_{\alpha}) & \text{if } r_{\alpha} \in MT. \end{cases} \quad (17)$$

Here, $V_{\mathbf{G}}$ and $V_{\ell m}^{\alpha}(r_{\alpha})$ can be decided by electron density.

The process for solving KS equation

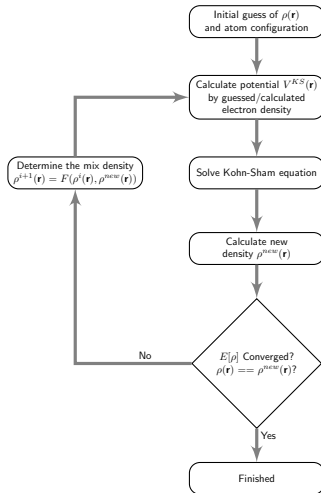


Figure 20 : Flow chart of the $(i + 1)$:th iteration for solving KS equation.

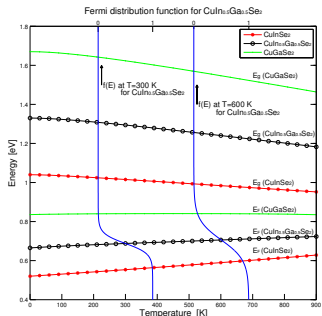


Figure 21 : Band-gap energy and Fermi energy for $1 \leq T \leq 900$ K of intrinsic CuInSe_2 , $\text{CuIn}_{0.5}\text{Ga}_{0.5}\text{Se}_2$, and CuGaSe_2 , determined from the fbp. The Fermi distribution $f(E)$ of $\text{CuIn}_{0.5}\text{Ga}_{0.5}\text{Se}_2$ is presented for $T = 300$ K and 600 K.

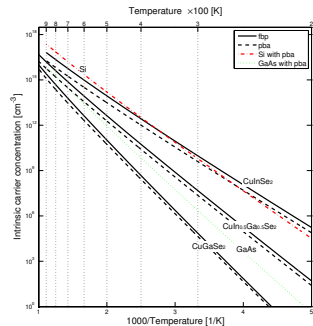


Figure 22 : Intrinsic carrier concentration as function of temperature. For comparison, the theoretical results for GaAs and Si using the pba are given.

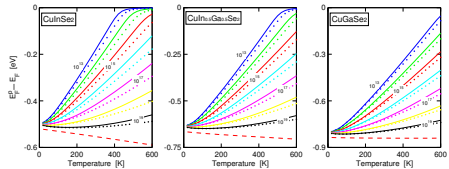


Figure 23 : Fermi level as function of the temperature $20 \leq T \leq 600$ of *p*-type CuInSe_2 , $\text{CuIn}_{0.5}\text{Ga}_{0.5}\text{Se}_2$, and CuGaSe_2 for the effective doping concentration $N_A = 10^{13}, 10^{14}, 10^{15}, ., \text{ and } 10^{19}$ acceptors cm^{-3} . Dashed lines represent the VBM with respect to the intrinsic Fermi level. Solid and dotted lines represents the fbp and the pba, respectively.

